ADVANCED FUNCTIONAL MATERIALS
www.afm-journal.de

Three-Dimensional Branched Nanowire Heterostructures as Efficient Light-Extraction Layer in Light-Emitting Diodes

Byeong Uk Ye, Buem Joon Kim, Joonmo Park, Hu Young Jeong, Jae Yong Park, Jong Kyu Kim, Jin-Hoe Hur, Myung Hwa Kim, Jong-Lam Lee, and Jeong Min Baik**

A facile method to fabricate three-dimensional branched ZnO/MgO nanowire heterostructures and their application as the efficient light-extraction layer in light-emitting diodes are reported. The branched MgO nanowires are produced on the hydrothermally-grown ZnO nanowires with a small tapering angle towards the tip (≈6°), by the oblique angle flux incidence of MgO. The structural evolution during the growth verifies the formation of the MgO nanoscale islands with strong (111) preferred orientation on very thin (5–7 nm) MgO (110) layer. The MgO nanobranches, then grown on the islands, are polycrystalline consisting of many grains oriented in specific directions of <200> and <220>, supported by the nucleation theory. The LEDs with the branched ZnO/MgO nanowire arrays show a remarkable enhancement in the light output power by 21% compared with that of LEDs with pristine ZnO nanowires. Theoretical calculations using a finite-difference time-domain method reveal that the nanostructure is very effective in breaking the wave-guiding mode inside the ZnO nanowires, extracting more light especially in radial direction through the MgO nanobranches.

1. Introduction

Recently, three-dimensional branched nanowire heterostructures have attracted much interest because of the unique and interesting optical, electronic, and catalytic properties.[1–8] Because of the high surface-to-volume ratio, the direct conduction pathway for charge transport, and the low reflectance induced by light scattering and trapping, the structures are especially attractive in a number of energy related applications, such as supercapacitors, batteries, photochemical cells, and solar cells.[5–8]

Light emitting diodes (LEDs) may also offer significant promise for reducing energy usage in lighting and display applications. In particular, GaInN-based vertical LEDs fabricated by laser the lift-off (LLO) technique are suitable for high power applications including the general illumination due to their excellent thermal and optical properties.[9,10] Limited light-extraction efficiency, originated from the total internal reflection (TIR) between the LED and surrounding medium, is currently one of the important subjects of intense research, as it retards the advancement of solid-state lighting which is just starting to supplant fluorescent as well as incandescent lighting.[11] Until now, various methods have been suggested to improve the light extraction efficiency such as surface roughening or texturing by photochemical etching or dry etching, introducing anti-reflection coatings and reflective mirrors, and so forth.[12–17] Hydrothermally grown 1D nanostructures are also expected to be attractive alternatives for extracting more light into the surrounding.[18,19] Recently, nanowire LEDs showed a drastic improvement in the light extraction (up to 79% at = 460 nm) by effective elimination of guided modes enabled by reducing the rod diameter to a sub-confinement regime.[20] However, these attractive effects originating from size reduction (<100 nm) of one-dimensional nanostructures are poorly practical. A quantum dot embedded in a nanowire can also enhance the light extraction efficiency, however, the efficiency may be limited by the fabrication imperfection and conventional photolithography is also not available.[21–23]

Here, we demonstrate a novel strategy based on 3D branched nanowire heterostructures for the enhancement in the light extraction of vertical LEDs with no efforts

B. U. Ye, Dr. J. Park, Prof. J. M. Baik
School of Mechanical and
Advanced Materials Engineering
KIST-UNIST-Ulsan Center for Convergent Materials
Ulsan National Institute of Science and
Technology (UNIST)
Ulsan 689–798, Korea
E-mail: jbaik@unist.ac.kr
B. J. Kim, J. Y. Park, Prof. J. K. Kim, Prof. J.-L. Lee
Department of Materials Science and Engineering
Division of Advanced Materials Science
Pohang University of Science and Technology (POSTECH)
Pohang, Gyeongbuk 790–784, Korea
E-mail: jllee@postech.ac.kr
Prof. H. Y. Jeong
UNIST Central Research Facilities (UCRF)
Ulsan National Institute of Science and Technology (UNIST)
Ulsan 689–798, Korea
J.-H. Hur
UNIST-Olympus Biomed Imaging Center (UOBC)
Ulsan National Institute of Science and Technology (UNIST)
Ulsan 689–798, Korea
Prof. M. H. Kim
Department of Chemistry & Nano Science
Ewha Womans University
Seoul 120–750, Korea

DOI: 10.1002/adfm.201303914

to synthesize the nanostructures with ultrasmall down to 100 nm for decreasing TIR. Until now, there are so many efforts to fabricate such branched nanostructures. However, most of them have focused on the catalyst-assisted growth by using the catalysts such as Au to grow the branched nanowires on the nanowire backbones.[24,25] Although these methods enable the growth of the highly-dense branched nanowires and so, may be widely used, but the processes may be complicated and the catalysts may contaminate the branched nanowires and the nanowire backbones. In this paper, we suggest a facile method to grow 3D branched nanowire heterostructures by combining bottom-up and top-down approaches. Under the appropriate growth conditions, the ZnO nanowires with a small tapering angle towards the tip (≈6°) are vertically grown on GaN substrate by hydrothermal method. The tapered nanowires enabled the oblique angle flux incidence of MgO on ZnO nanowires, which enhanced atomic shadowing by initial MgO nuclei and created the branch-shaped nanostructures. ZnO/TiO_2 branched structures could be also produced by the same method. Finally, V-LEDs with the nanostructures provided 21% more light output power compared to those with only ZnO nanowires. This achievement is attributed to the effective reduction of TIR and the guided modes, caused by the branch-shaped nanostructures, in good agreement with theoretical calculations using a 3-dimensional finite-difference time-domain (FDTD) method.

2. Results and Discussion

Figure 1a shows the fabrication procedure for 3D ZnO/MgO branched nanowire arrays. Schematic diagrams of the V-LEDs fabrication process are shown in Figure 1a. The ZnO nanowires with a small tapering angle towards the tip (≈6°) grow vertically to 2.5 μm in length and the diameter continuously reduce from 500 to 200 nm along the body of the nanowires from the bottom to the top, as shown in Figure 1b. The electron-beam evaporation of MgO produces branch-shaped nanostructures, in which MgO nanowires with a diameter of 10–20 nm and an angle of approximately 57° respect to the vertical direction to the substrate are grown on the side facet of ZnO nanowires. They appear to be tight and uniform along the body of the nanowires and mushroom-like features on the top of the nanostructures are shown. By the same method, ZnO/TiO_2 branched structures can be produced, also seen in Figure 1b.

Figures 2a–e shows the tilted view and cross-sectional images of branch-shaped nanostructures with MgO thickness from 20 nm to 2 μm. When 20-nm-thick MgO is deposited on ZnO, MgO islands less than 10 nm in size are produced. As the thickness increases to 50 nm (Figure 2b), the MgO nanobranches with length of 50 nm are clearly shown, even at the bottom area of the nanowires. A little difference in the length of MgO nanobranches between left and right sides of the ZnO nanowires can be solved by the well-control of the deposition

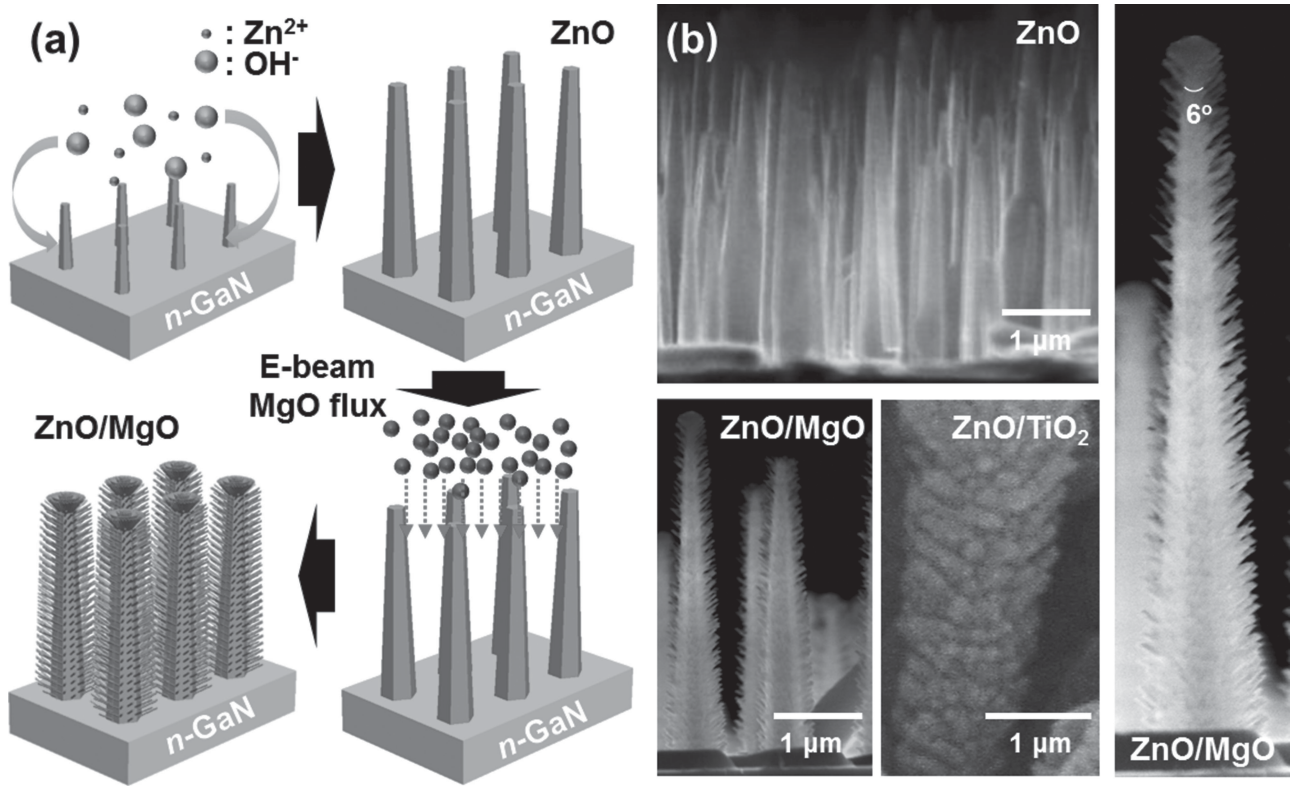

Figure 1. a) Fabrication procedure for 3D ZnO/MgO branched nanowire arrays. After ZnO nanowires growth, the MgO is evaporized to the nanowires at room temperature. b) SEM image of the ZnO nanowires and hierarchical ZnO/MgO nanostructures, in which MgO nanowires with average diameter of 10–20 nm. ZnO/TiO_2 nanostructures are also shown.

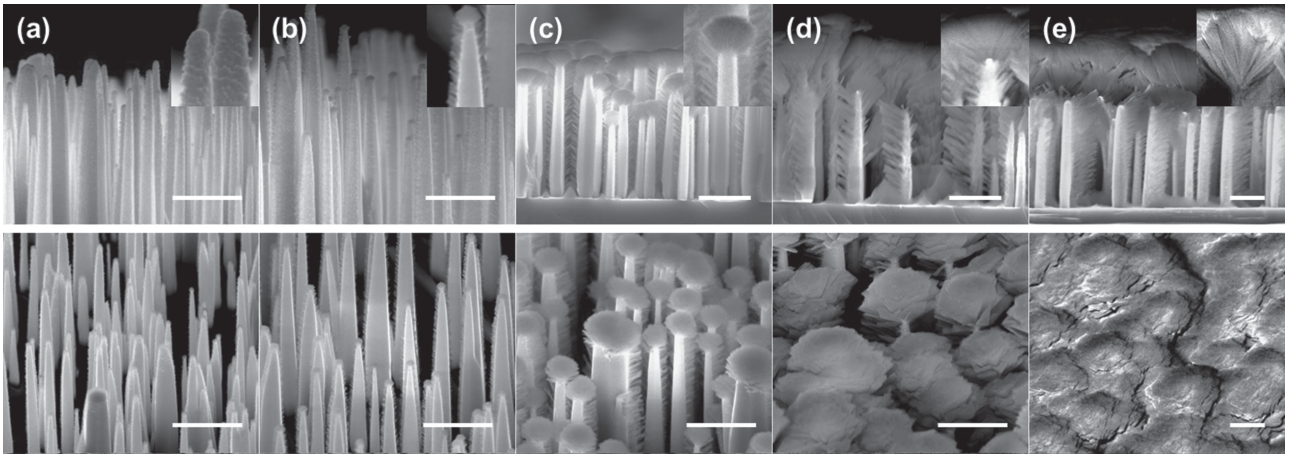

Figure 2. SEM images show the tilt (45°) and the cross-section of the MgO nanobranches grown by e-beam evaporation; MgO mass thickness is a) 20 nm, b) 50 nm, c) 200 nm, d) 500 nm, and e) 2 μm. Note that mushroom-like MgO starts to be produced on the top of the ZnO nanowires. Further increase in the thickness of MgO increase the length of the MgO nanobranches and the size of the mushrooms. (scale bar = 1 μm).

angle. Note that mushroom-like MgO starts to be produced on the top of the ZnO nanowires. Further increase in the thickness of MgO increase the length of the MgO nanobranches and the size of the mushrooms. Eventually, the neighboring mushrooms are connected over a long face and the MgO completely cover the ZnO nanowires at 2-μm-thick MgO, leaving the void space among the nanostructures.

The crystal structures of the hierarchical branched-nanostructures were characterized by low-magnified bright-field (BF) TEM and high-resolution TEM (HR-TEM) images, as shown in **Figure 3**. As shown in Figure 3a,b, MgO nanobranches are clearly visible, with a diameter of 10–30 nm. It is also seen that the mushroom at the top region consists of many MgO nanowires. Figure 3c shows that before the growth

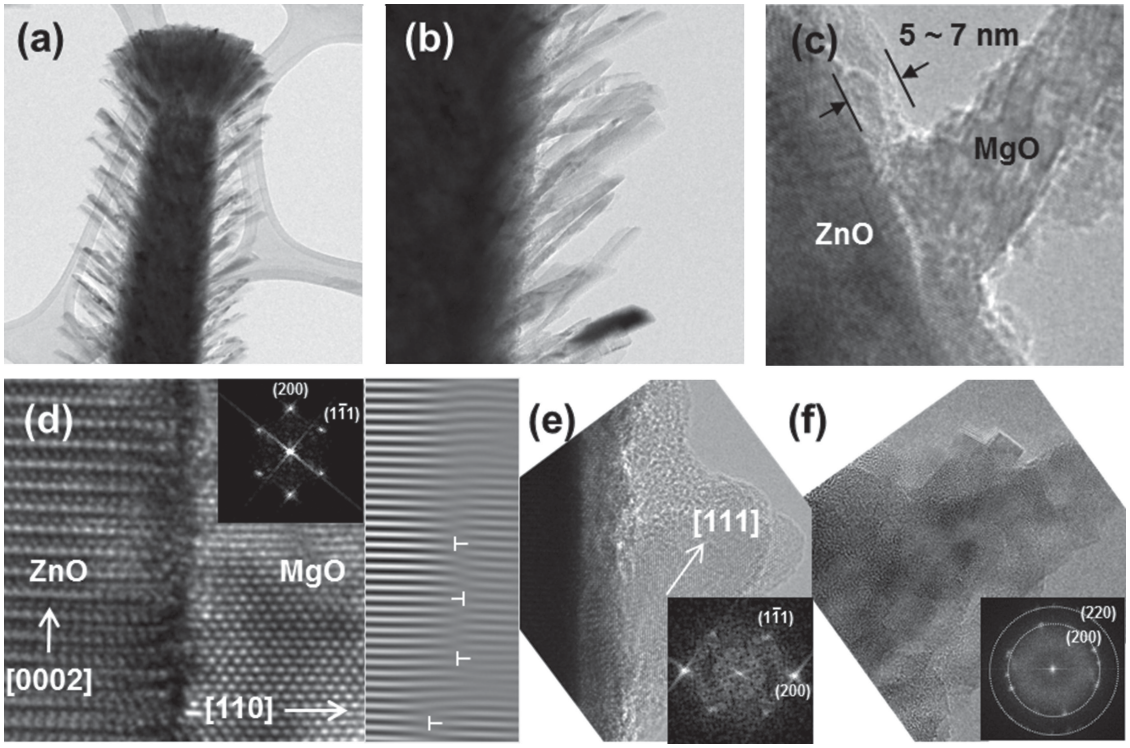

Figure 3. Transmission electron microscopy (TEM) images of a hierarchical ZnO/MgO nanostructure. a,b) Low-magnification images of single ZnO/MgO nanostructure c) Low-magnification image at the interface between the ZnO and MgO layer. Before the growth of the MgO nanobranches, very thin (5–7 nm) MgO layer is formed on the surface. d) High-resolution TEM (HR-TEM) images at the interface region of ZnO and MgO and Fourier filtering image toward the [0002] direction. e) The MgO cluster with (111) preferred orientation. f) HR-TEM image of a MgO nanobranch.

of the MgO nanobranches, very thin (5–7 nm) MgO layer is formed on the surface. From the HR-TEM imaging (Figure 3d) at the interface region of ZnO and MgO, the nearly epitaxial growth of MgO (110) film on M-plane ZnO ($10\bar{1}0$) with an interface is clearly demonstrated. Indeed, high magnification at the interface region clearly shows the crystalline continuity between the substrate and the thin film, except the presence of a few dislocations at the interfacial region, shown by the Inverse Fast Fourier filtered image by selecting ZnO (0002) and MgO (200), probably due to the lattice mismatch between both structures.[26] As the MgO thickness increases, the MgO cluster with (111) preferred orientation with lattice spacing of 0.243 nm was clearly shown. Previously, the change of the preferred orientation was reported to be due to the strong polarity induced by the Mg^{2+} plane and the O^{2-} plane in the (111) orientation of the MgO, which increases the sticking probability of adatoms on the polar surface.[27] The further increase in the MgO thickness promotes the preferred growth of the MgO, producing the nanowire-shaped branches. The TEM image and the corresponding diffraction pattern reveal that the MgO nanowire is poly-crystalline, consisting of many grains.

The preferred growth of the MgO nanobranches on the sidewall of the ZnO nano can be explained as follows. On GaN substrate, the ZnO nanowires are usually grown vertically (Figure 1). Due to the tapered geometry of the ZnO nanowires, the MgO vapor flux during the subsequent e-beam evaporation is thus obliquely incident with an angle of approximately $\alpha = 87$ ° with respect to the m-plane of the ZnO nanowires, as shown in **Figure 4**. Highly oblique MgO vapor flux incidence enhances atomic shadowing by initial MgO nuclei and creates inclined columnar structures. The direction (β) of the nanostructures with the respect to the substrate (here, the substrate is ZnO m-plane) is critically dependent on the angle of incident vapor flux.[28] To investigate the shadow effect, we grew the ZnO nanowires on the ZnO hemispheres, which can change the growth direction of the nanowires. The hemispheres were synthesized by a spin coating method of polystyrene spheres, followed by the deposition of ZnO film by a RF sputtering method and heating at 300 °C for 1 h in air. **Figure 5** is a SEM image of the ZnO nanowires grown on the hemispheres. Most nanostructures show branch-shaped morphologies irrespective of the growth direction of the ZnO nanowires and the β decreases as α decrease. However, when MgO is incident at low angle of 33.6°, a film-type MgO branch is observed, as shown in the inset (see the left image) this means that the nanobranches are produced due to the shadow effects. The nanobranches are also formed when the TiO_2 is deposited onto the ZnO nanowires (see the right image in the inset).

The growth mechanism of MgO nanobranches on ZnO nanowires can be summarized in Figure 4. MgO (110) film on ZnO ($10\bar{1}0$) plane with an atomically sharp interface and the presence of a few stacking faults is grown below 5–7 nm due to the small lattice mismatch (≈4.9%). Strong (111) preferred orientation of MgO islands is developed as the thickness increases due to the strong polarity of (111) orientation, producing shadowed regions. MgO nanobranches, in polycrystalline consisting of many grains oriented in specific directions of <200> and <220>, are then grown by the oblique angle flux incidence of MgO, in which the angle (β) of the branches critically depends on the angle flux incidence. According to the nucleation theory, the critical radius (r^*) of the nucleation critically depends on the surface energy (γ) and volume energy (ΔGv), which is given by[29]

$$r^* = r_c = 2 \times \frac{\gamma}{G_v}$$

In this case, the critical thickness of the MgO (200) is about 0.3 nm, may be small enough for the nucleation during the e-beam evaporation.

It is well-known that the ZnO nanowires on GaN LEDs can enhance the light extraction efficiency by the refractive-index modulation. The light extraction efficiency is significantly dependent on the density and shape of the ZnO nanowires.[19]

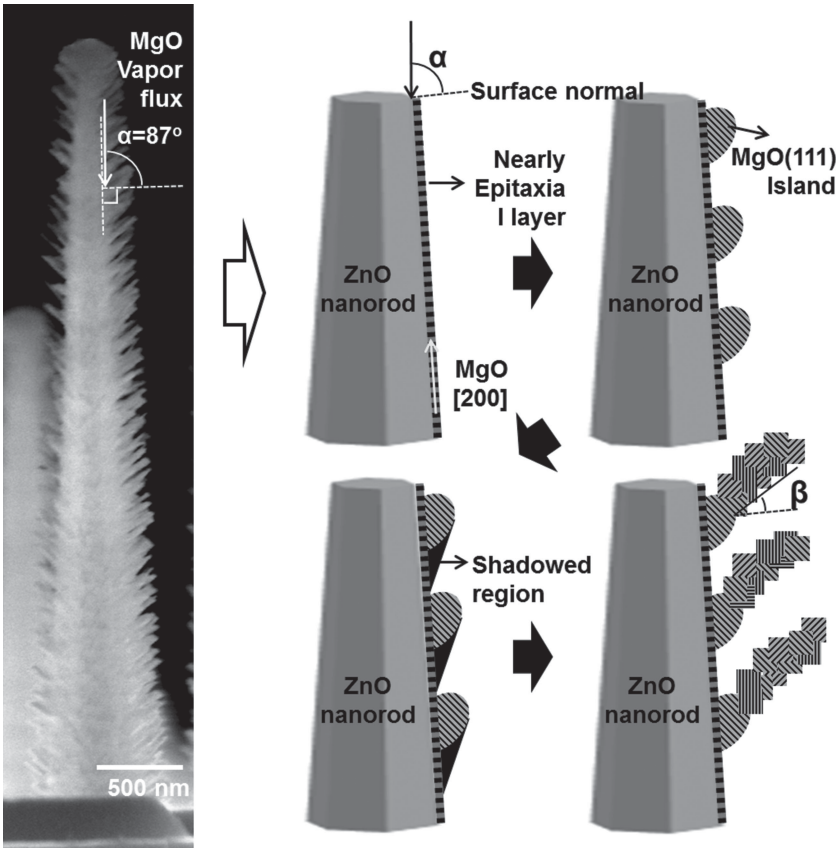

Figure 4. Simplified sketch of growth mechanism of MgO nanobranches on ZnO nanowire. The preferred growth of the MgO may be explained by the significant local non-uniformity by the shadowing in oblique incidence onto ZnO m-plane. High incident angle of MgO vapor flux (α).

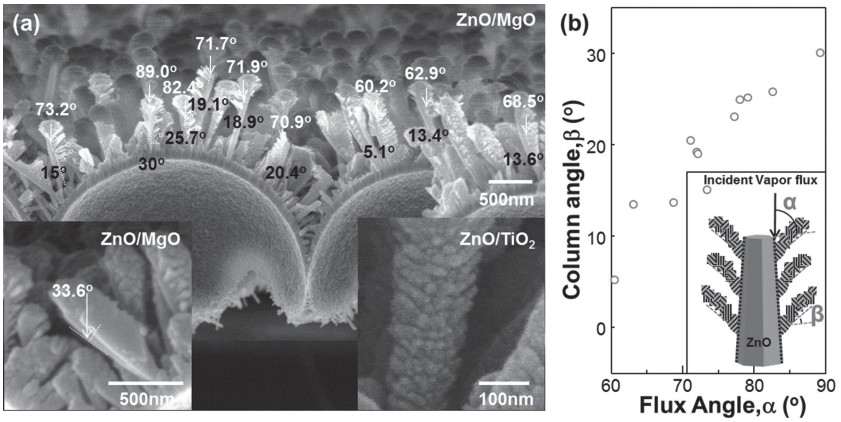

Figure 5. a) SEM image which shows that the direction of MgO nanobranches (β) decreases as the angle of incident vapor flux (α) decreases. Film-type MgO branch (as shown in inset, left image), The TiO_2 is deposited onto the ZnO nanowires (right image). b) The direction of MgO nanobranches (β) vs the angle of incident vapor flux (α).

Figure 6 shows that the EL intensity and the light output power of V-LEDs increases up to 21% as the thickness of MgO layer increased up to 0.5 μm, compared to V-LEDs with ZnO/n-GaN layer. The forward voltages of V-LEDs with the n-GaN/ZnO and n-GaN/ZnO/MgO layers at an injection current of 20 mA are 2.81 V and 2.79 V, respectively (Figure 2S, Supporting Information). Furthermore, the reverse leakage currents of V-LEDs are almost same before and after MgO deposition. Further increase in thickness of MgO layer to 2.0 μm caused reduction of light output power. For thicker MgO than 0.5 μm, the MgO top layer are connected over a long face, leaving the void space among the nanowires. This might imply that the light extracted through the MgO nanowires to the void space can be reflected by the MgO top layer and enter into GaN layer. Figure 3S (Supporting Information) shows the transmittance as a function of the MgO layer thickness, measured using an integrating sphere. Transmittance enhancement ratio is defined as $T_{\text{ratio}}(\%) = \frac{T_{\text{MgO/ZnO/GaN}}}{T_{\text{ZnO/GaN}}} \times 100 - 100$. Due to the Fabry-Perot oscillations in transmittance spectra,[30] average value in the wavelength range from 440 nm to 470 nm was used, corresponding to the peak wavelength of InGaN blue LEDs. The 0.5-μm-thick MgO layer showed high enhancement ratio of 11.4% originated from the MgO branch-shaped nanostructure. As the thickness of MgO layer exceeds 0.5 μm, the enhancement ratio decreases.

The photons generated in the active region propagate within the ZnO nanowires until the light is extracted out of the hexagonal top facet, as explained by the wave-guiding effect, due to the large refractive index difference between ZnO (n = 2.1) and air (n = 1).[31,32] The CSEM images (right images) in **Figure 7** clearly demonstrates the wave-guiding phenomenon through the nanowires.[33–37] Although some light is also emitted out of the side facet, the intensity is not as great as that from the top facet. On the contrary, for the hierarchical ZnO/MgO structure, the intensity of the light emitted out of the side facet near the bottom area of the nanowire is same or even higher than that of the light extracted out of the hexagonal top. The movie also shows that the light is emitted in all directions from the ZnO/MgO nanostructures, while the light is emitted from the top and bottom facets of the ZnO nanowires. This ascribes to the refractive index modulation of ZnO/MgO hierarchical nanostructures. According to the effective medium approximation,[38] the effective refractive index is calculated to be 1.45, smaller than that (≈1.7) of MgO film, by assuming that the porosity of MgO nanobranches is about P = 72%. This increases the critical angle for TIR and thus more lights are able to enter to the MgO layer. The MgO nanowires are

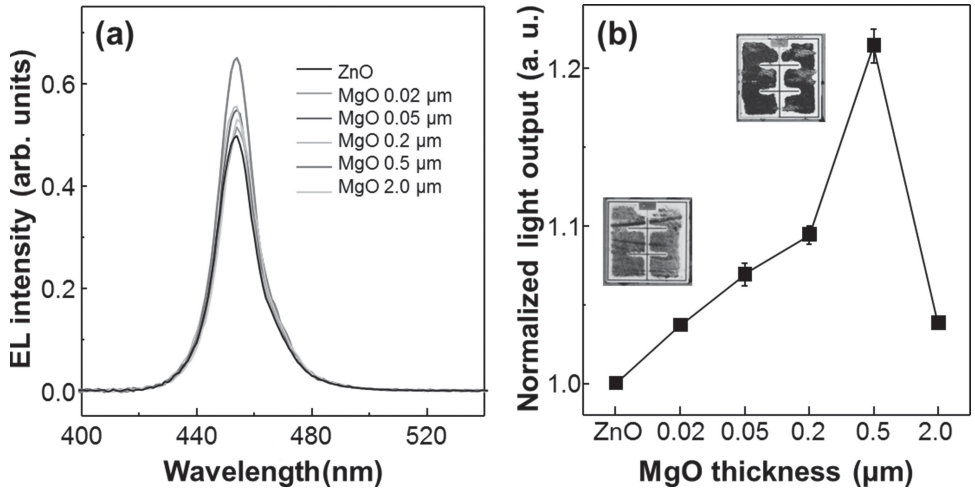

Figure 6. a) EL spectra of ZnO/n-GaN and ZnO/MgO/n-GaN at 20 mA. b) The light output power of V-LEDs with MgO thickness. The power increases up to 21% as the thickness of MgO layer increased up to 0.5 μm, compared to V-LEDs with n-GaN/ZnO layer. Optical microscopy images of n-GaN/ZnO n-GaN/ZnO/MgO.

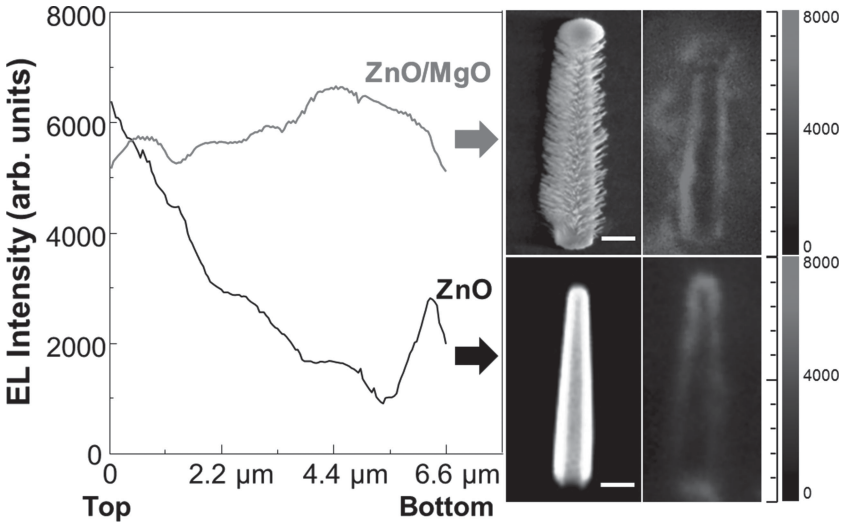

Figure 7. EL intensity of LEDs with ZnO nanowires and ZnO/MgO nanostructures along the nanostructures from the top to bottom region. CSEM images (right images) are also shown on the right side. (scale bar = 1 μm).

also able to enhance the light extraction at the MgO/air interface because the roughened surface reduces internal light reflection.

In order to estimate the effect of such a unique geometry of the ZnO/MgO nanostructures on the far field emission pattern and the electric-field distribution for V-LEDs, 3-dimensional FDTD simulations were performed. **Figure 8**a shows that the schematic V-LED structure used in the FDTD calculation composed of a 300 nm thick Ag reflector, a 200 nm p-GaN layer, a 100 nm InGaN/GaN MQW active layer and a 1.5 μm thick n-GaN layer. Two structures, a ZnO nanowire (500 nm diameter and 3 μm height) and a ZnO nanowire with MgO branches (50 nm diameter, 500 nm length), on the V-LED were simulated. The electric point dipole in the center of the InGaN MQW active layer is regarded as the light source. Boundary condition for the FDTD simulation is set to perfect matched layer (PML) to avoid the reflected electromagnetic wave at the edge of the structure and it consists of a perfect electric conductor (PEC) plane as bottom layer. FDTD simulation were then performed during the light propagation over a distance d = 45 μm to reach steady state. Cross-sectional discrete Fourier transform (DFT) monitor

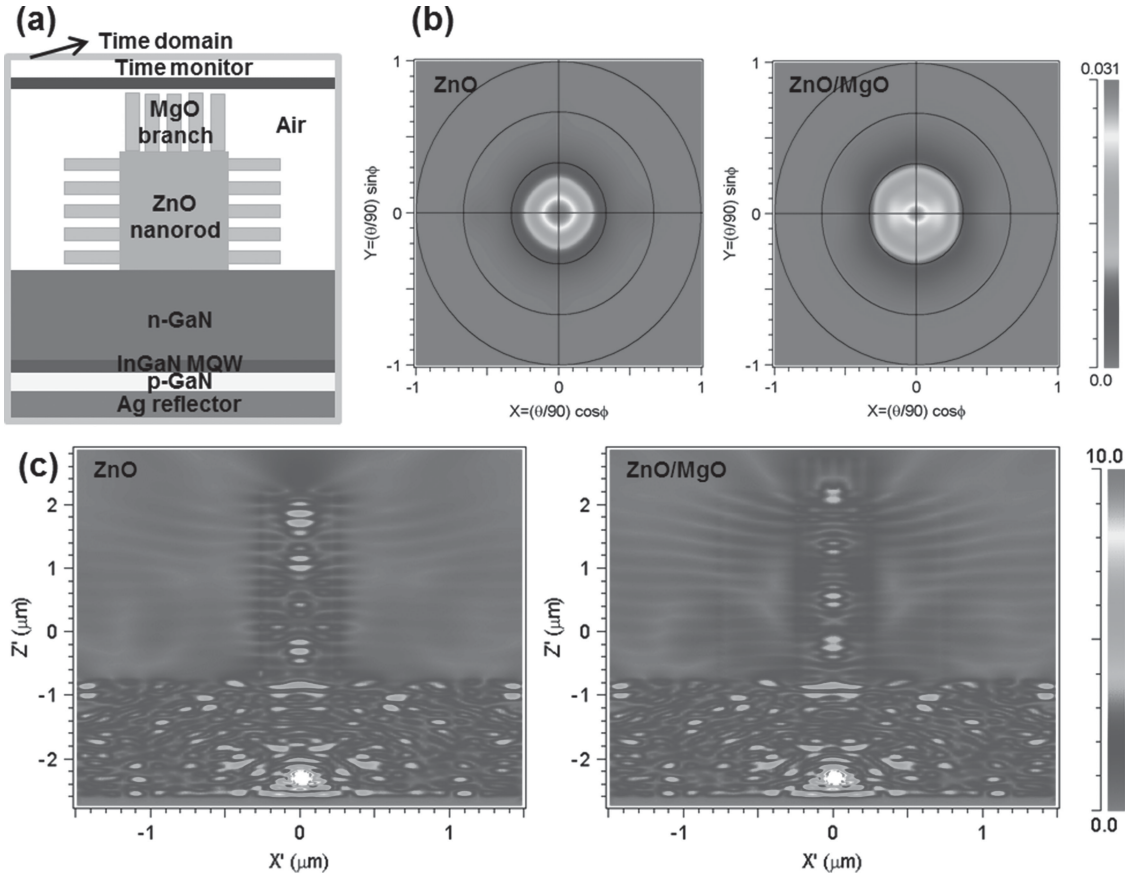

Figure 8. a) Schematic structure of the V-LEDs with ZnO nanowire/MgO branch for numerical analysis. b) Simulated polar projection of far-field intensity for the ZnO nanowire on n-GaN and ZnO nanowire/MgO branch on n-GaN in V-LEDs. c) The electric field intensity for a cross section with each structure in the x–z plane at λ = 450 nm, which corresponds to a blue LEDs.

was used to get the spatial electric field distribution. Figure 8b shows far field emission patterns of the ZnO nanowire and the ZnO/MgO hierarchical nanostructure on the V-LED. For the ZnO nanowire, strong far-field emission intensity is observed at the center of the rod indicating that the electromagnetic wave (EM) propagates along the *z*-axis within the ZnO nanowire due to the wave-guiding effect, which is consistent with Figure 7. On the other hand, the far-field emission intensity at the center of the ZnO/MgO branched nanostructure is not as strong as observed for the ZnO reference, rather a flower-like emission pattern with a six-fold symmetry is observed outside the nanostructure, which means that the EM waves are effectively "leaking" out of the ZnO nanowire through the MgO branches breaking the wave-guiding mode. Such remarkable changes can be clearly seen in the electric-field distribution as shown in Figure 8c. The electric field distribution outside the nanowire is much more dynamic for the ZnO/MgO hierarchical nanostructure with higher amplitude that that for the ZnO nanowire. In addition, the amplitude of the electric field inside the ZnO nanowire decreases as the EM wave propagates through the ZnO/MgO hierarchical nanostructure whereas that does not change remarkably for the ZnO nanowire, which indicates that the hierarchical nanostructures are very effective in light extraction by breaking the wave-guiding mode.

3. Conclusion

We reported a facile method to grow 3D branched nanowire heterostructures by combining bottom-up and top-down approaches. Under the appropriate growth conditions, the ZnO nanowires with a small tapering angle towards the tip (≈6°) are vertically grown on GaN substrate by hydrothermal method. The tapered nanowires enabled the oblique angle flux incidence of MgO on ZnO nanowires by the e-beam evaporation at room temperature, which enhanced atomic shadowing by initial MgO nuclei and created the branch-shaped nanostructures. The high-resolution TEM analysis shows that the MgO nanobranches are grown on the MgO nanoscale islands with strong (111) preferred orientation on very thin (5–7 nm) MgO (110) layer. The MgO nanobranches are polycrystalline consisting of many grains oriented in specific directions of <200> and <220>, supported by the nucleation theory. The LEDs with the ZnO/MgO 3D branched nanowire heterostructures show a remarkable enhancement in the light output power by 21% compared with that of LEDs with pristine ZnO nanowires. Theoretical calculations using a finite-difference time-domain method reveal that the nanostructure is very effective in breaking the wave-guiding mode inside the ZnO nanowires, extracting more light especially in radial direction through the MgO nanobranches.

4. Experimental Section

Fabrication of Vertical Light Emitting Diode: A 500-nm-thick undoped GaN buffer layer, a 2-μm-thick n-type GaN, an InGaN/GaN MQW active region, a p-type GaN layer were grown in sequence on c-plane sapphire substrates using metal-organic chemical vapor deposition. For the fabrication of V-LEDs (1 mm × 1 mm), Ag-based reflective p-type ohmic contact was deposited on the p-type GaN, followed by annealing at 400 °C for 2 min in air ambient. And the wafer was bonded to the Si substrate by a thermo-compressive bonding process at 320 °C using Au–Sn bonding layers. Subsequently, the sapphire substrate was separated using KrF pulsed excimer laser. After the LLO process, undoped GaN was removed and SiO_2 passivation layer and Cr/Au n-type ohmic contact were deposited on the n-type GaN, forming n-side-up vertical InGaN LEDs on the Si wafer.

Growth of Branch-Shaped Nanostructures: ZnO nanowires arrays were grown on the N-face n-type GaN surface of the V-LEDs. Before the growth, the substrates are exposed to UV radiation and ozone for 30 min to enhance the growth of the nanowires. The V-LEDs are loaded into Teflon-sealed stainless autoclave and were put facing down on the nutrient growth solution (1:1 ratio of zinc nitrate and hexamethylenetetramine (HMTA) 20 mM) and was kept in an oven at 90°C for 3 h. The autolcave was then taken out from the oven and immersed in a cold water bath in order to increase the cooling rate. After that, the V-LEDs were removed from the aqueous solutions, rinsed with distilled water. The V-LEDs sample was then loaded into an e-beam evaporator to form MgO layer. MgO (20 nm to 2 μm mass thick) layer was evaporated using high purity MgO pellet (99.99% with a diameter of 3 mm) at a base pressure of 3.0×10^{-6} Torr and room temperature. The deposition rate was fixed to be approximately 2 nm s^{-1}. The voltage was set to be 6 kV.

Measurement of Light Output Power of V-LEDs and the Characterization of the Branch-Shaped Nanostructures: The light output power of V-LEDs was measured at an unpacked (on-wafer) configuration using an integrating sphere. The scanning electron microscopy (SEM) was done using a PHILIPS XL30S with an accelerating voltage of 5 kV. The high-resolution transmission electron microscopy (HRTEM) images were collected using a Cs-corrected JEM-2100 operated at 200 kV. The confocal scanning electroluminescence microscopy (CSEM) was done using a IX81 Motorized Microscope with a spatial resolution of 250 nm. where it was finally detected using a cooled charge coupled device (CCD) detector (iXon3 888).

Supporting Information

Supporting Information is available from the Wiley Online Library or from the author.

Acknowledgements

B.U.Y. and B.J.K. contributed equally to this work. This work was supported by the IT R&D program of MKE/KEIT [10035598, 180 lm/W High-efficiency nano-based LEDs], by the Pioneer Research Center Program through the National Research Foundation of Korea funded by the Ministry of Science, ICT & Future Planning (NRF-2013M3C1A3063602), and by the Future Strategic Fund(1.130061.01) of UNIST(Ulsan National Institute of Science and Technology).

Received: November 20, 2013
Revised: December 17, 2013
Published online: February 13, 2014

[1] C. Cheng, H. J. Fan, *Nano Today* **2012**, *7*, 327.
[2] M. Bierman, S. Jin, *Energy Environ. Sci.* **2009**, *2*, 1050.
[3] X. Liu, Y. Lin, S. Zhou, S. Sheehan, D. Wang, *Energies* **2010**, *3*, 285.
[4] S. Wang, Y. Yu, Y. Zuo, C. Li, J. Yang, C. Lu, *Nanoscale* **2012**, *4*, 5895.
[5] S. H. Ko, D. Lee, H. W. Kang, K. H. Nam, J. Y. Yeo, S. J. Hong, C. P. Grigoropoulos, H. J. Sung, *Nano Lett.* **2011**, *11*, 666.
[6] A. Kargar, K. Sun, Y. Jing, C. Choi, H. Jeong, G. Y. Jung, S. Jin, D. Wang, *ACS Nano* **2013**, *7*, 9407.

[7] I. S. Cho, Z. Chen, A. J. Forman, D. R. Kim, P. M. Rao, T. F. Jaramillo, X. Zheng, *Nano Lett.* **2011**, *11*, 4978.
[8] X. Sun, Q. Li, Y. Lü, Y. Mao, *Chem. Commun.* **2013**, *49*, 4456.
[9] H. W. Jang, S. W. Ryu, H. K. Yu, S. H. Lee, J.-L. Lee, *Nanotechnology* **2010**, *21*, 025203.
[10] S. J. Wang, K. M. Uang, S. L. Chen, Y. C. Yang, S. C. Chang, T. M. Chen, C. H. Chen, B. W. Liou, *Appl. Phys. Lett.* **2005**, *87*, 011111.
[11] E. F. Schubert, Light Emitting Diodes, 2nd Ed., Cambridge University Press, Cambridge, UK **2006**.
[12] T. Fujii, Y. Gao, Sharma, E. L. Hu, S. P. DenBaars, S. Nakamura, *Appl. Phys. Lett.* **2004**, *84*, 855.
[13] M. Megens, A. David, J. J. Wierer, *Nat. Photonics* **2009**, *3*, 163.
[14] J. K. Kim, S. Chhajed, M. F. Schubert, E. F. Schubert, A. J. Fischer, M. H. Crawford, J. Cho, H. Kim, C. Sone, *Adv. Mater.* **2008**, *20*, 801.
[15] H. Jia, L. Guo, W. Wang, H. Chen, *Adv. Mater.* **2009**, *21*, 4641.
[16] H. M. Kim, D. S. Kim, Y. S. Park, D. Y. Kim, T. W. Kang, K. S. Chung, *Adv. Mater.* **2002**, *14*, 991.
[17] J.-Q. Xi, H. Luo, A. J. Pasquale, J. K. Kim, E. F. Schubert, *IEEE Photonics Technol. Lett.* **2006**, *18*, 2347.
[18] X. Liu, W. Zhou, Z. Yin, X. Hao, Y. Wu, X. Xu, *J. Mater. Chem.* **2012**, *22*, 3916.
[19] K.-K. Kim, S.-D. Lee, H. Kim, J.-C. Park, S.-N. Lee, Y. Park, S.-J. Park, S.-W. Kim, *Appl. Phys. Lett.* **2009**, *94*, 071118.
[20] M.-L. Kuo, Y.-S. Kim, M.-L. Hsieh, S.-Y. Lin, *Nano Lett.* **2011**, *11*, 476.
[21] M. E. Reimer, G. Bulgarini1, N. Akopian1, M. Hocevar1, M. B. Bavinck1, M. A. Verheijen, E. P. Bakkers, L. P. Kouwenhoven, V. Zwiller, *Nat. Commun.* **2012**, *3*, 737.
[22] T. Heindel, C. Schneider, M. Lermer, S. H. Kwon, T. Braun, S. Reitzenstein, S. Höfling, M. Kamp, A. Forchel, *Appl. Phys. Lett.* **2010**, *96*, 011107.
[23] N. Gregersen, T. R. Nielsen, J. Mørk, J. Gérard, J.-M. Claudon, *Opt. Express* **2010**, *18*, 21204.
[24] K. A. Dick, K. Deppert, M. W. Larsson, T. Martensson, W. Seifert, L. R. Wallenberg, L. Samuelson, *Nat. Mater.* **2004**, *3*, 380.
[25] D. Wang, F. Qian, C. Yang, Z. H. Zhong, C. M. Lieber, *Nano Lett.* **2004**, *4*, 871.
[26] S. M. Bobade, *Appl. Phys. Lett.* **2012**, *100*, 072102.
[27] H. K. Yu, J.-L. Lee, *Cryst. Growth Des.* **2010**, *10*, 5200.
[28] Y.-P. Zhao, D.-X. Yeb, G.-C. Wangb, T.-M. Lub, *Nanotubes Nanowires* **2003**, *5219*, 59.
[29] W. D. Callister, D. G. Rethwisch, Materials Science and Engineering. 8th Ed, John Wiley and Sons, Inc., New York **2011**.
[30] B. Harbecke, *Appl. Phys. B.* **1986**, *39*, 165.
[31] J. Zhong, H. Chen, G. Saraf, Y. Lu, C. K. Choi, J. J. Song, D. M. Mackie, H. Shen, *Appl. Phys. Lett.* **2007**, *90*, 203515.
[32] C. H. Chao, W. H. Lin, W. H. Chen, C. H. Changjean, C. F. Lin, *Semicond. Sci. Technol.* **2009**, *24*, 105017.
[33] K. S. Kim, S.-M. Kim, H. M. Jeong, S. Jeong, G. Y. Jung, *Adv. Funct. Mater.* **2010**, *20*, 1076.
[34] S.-M. Kim, K. S. Kim, G. Y. Jung, J. H. Baek, H. Jeong, M. S. Jeong, *J. Phys. D: Appl. Phys.* **2009**, *42*, 152004.
[35] S. H. Kim, H. H. Park, Y. H. Song, H. J. Park, J. B. Kim, S. R. Jeon, H. Jeong, M. S. Jeong, G. M. Yang, *Opt. Express* **2013**, *21*, 7125.
[36] H. G. Kim, T. V. Cuong, H. Jeong, S. H. Woo, O. H. Cha, E.-K. Suh, C.-H. Hong, H. K. Cho, B. H. Kong, M. S. Jeong, *Appl. Phys. Lett.* **2008**, *92*, 061118.
[37] Y. J. Park, H. Y. Kim, J. H. Ryu, H. K. Kim, J. H. Kang, N. Han, M. Han, H. Jeong, M. S. Jeong, C.-H. Hong, *Opt. Express* **2011**, *19*, 2029–2036.
[38] M. Riley, A. Redo-Sanchez, P. Karampourniotis, J. Plawsky, T.-M. Lu, *Nanotechnology* **2012**, *23*, 325301.